

***Arabidopsis* SET DOMAIN GROUP2 Is Required for H3K4 Trimethylation and Is Crucial for Both Sporophyte and Gametophyte Development**

Alexandre Berr,^a Emily J. McCallum,^{a,1} Rozenn Ménard,^a Denise Meyer,^a Jörg Fuchs,^b Aiwu Dong,^c and Wen-Hui Shen^{a,2}

^aInstitut de Biologie Moléculaire des Plantes du Centre National de la Recherche Scientifique, Université de Strasbourg, 67084 Strasbourg Cedex, France

^bLeibniz-Institute of Plant Genetics and Crop Plant Research, D-06466 Gatersleben, Germany

^cState Key Laboratory of Genetic Engineering, Department of Biochemistry, Institute of Plant Biology, School of Life Sciences, Fudan University, Shanghai 200433, PR China

Histone H3 lysine 4 trimethylation (H3K4me3) is abundant in euchromatin and is in general associated with transcriptional activation in eukaryotes. Although some *Arabidopsis thaliana* SET DOMAIN GROUP (SDG) genes have been previously shown to be involved in H3K4 methylation, they are unlikely to be responsible for global genome-wide deposition of H3K4me3. Most strikingly, sparse knowledge is currently available about the role of histone methylation in gametophyte development. In this study, we show that the previously uncharacterized *SDG2* is required for global H3K4me3 deposition and its loss of function causes wide-ranging defects in both sporophyte and gametophyte development. Transcriptome analyses of young flower buds have identified 452 genes downregulated by more than twofold in the *sdg2-1* mutant; among them, 11 genes, including *SPOROCTELESS/NOZZLE* (*SPL/NZZ*) and *MALE STERILITY1* (*MS1*), have been previously shown to be essential for male and/or female gametophyte development. We show that both *SPL/NZZ* and *MS1* contain bivalent chromatin domains enriched simultaneously with the transcriptionally active mark H3K4me3 and the transcriptionally repressive mark H3K27me3 and that *SDG2* is specifically required for the H3K4me3 deposition. Our data suggest that *SDG2*-mediated H3K4me3 deposition poises *SPL/NZZ* and *MS1* for transcriptional activation, forming a key regulatory mechanism in the gene networks responsible for gametophyte development.

INTRODUCTION

Histone methylation is one type of the epigenetic marks that play essential regulatory functions in the organization of chromatin structure and genome function (Yu et al., 2009; Liu et al., 2010). In general, active transcription depending on a permissive chromatin structure is associated with histone H3 lysine 4 (H3K4) and/or H3K36 methylation, whereas transcriptional repression is associated with H3K9 and/or H3K27 methylation. Enzymes catalyzing histone Lys methylation contain an evolutionarily conserved SET domain (Tschiersch et al., 1994), named after three proteins initially identified in *Drosophila melanogaster*: SuVar(3–9), E(z), and Trithorax. The *Arabidopsis thaliana* genome contains 47 SET DOMAIN GROUP (SDG) genes: *SDG1* to *SDG47* (<http://www.chromdb.org>), which could be classified into several

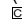
distinct phylogenetic groups (Baumbusch et al., 2001; Springer et al., 2003; Zhao and Shen, 2004; Ng et al., 2007). So far, only some SDG genes have been investigated for their roles in plant growth and development (reviewed in Yu et al., 2009; Liu et al., 2010); the biological functions of a larger number of SDG genes remain unknown.

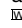
In *Drosophila*, Trithorax group (TrxG) SET domain proteins mediate H3K4 and/or H3K36 methylation and counteract transcriptional repression by Polycomb group (PcG)-mediated H3K27 methylation to sustain active expression of developmental regulatory genes (Schuettengruber et al., 2007). The TrxG family in *Arabidopsis* comprises 12 SDG genes, six of which have been assigned a biological function to date. Five of the six characterized genes, *SDG8/ASHH2/EFS/CCR1*, *SDG25/ATXR7*, *SDG26/ASHH1*, *SDG27/ATX1*, and *SDG30/ATX2*, are involved in flowering time regulation (Soppe et al., 1999; Kim et al., 2005; Zhao et al., 2005; Pien et al., 2008; Saleh et al., 2008; Xu et al., 2008; Berr et al., 2009; Tamada et al., 2009), whereas *SDG4/ASHR3* is involved in late stages of pollen development (Cartagena et al., 2008; Thorstensen et al., 2008). In addition, *ATX1* involved in H3K4 trimethylation (H3K4me3) is necessary for normal root, leaf, and floral organ growth (Alvarez-Venegas et al., 2003; Alvarez-Venegas and Avramova, 2005); and *SDG8/ASHH2/EFS/CCR1*, primarily involved in H3K36me2 and H3K36me3, is implicated in the regulation of organ size, shoot

¹Current address: Department of Biology, Plant Biotechnology, ETH Zürich, Universitätstrasse 2, 8092 Zurich, Switzerland.

²Address correspondence to wen-hui.shen@ibmp-cnrs.unistra.fr.

The author responsible for distribution of materials integral to the findings presented in this article in accordance with the policy described in the Instructions for Authors (www.plantcell.org) is: Wen-Hui Shen (wen-hui.shen@ibmp-cnrs.unistra.fr).

 Some figures in this article are displayed in color online but in black and white in the print edition.

 Online version contains Web-only data.

www.plantcell.org/cgi/doi/10.1105/tpc.110.079962

branching, fertility, and carotenoid composition (Soppe et al., 1999; Xu et al., 2008; Cazzonelli et al., 2009; Grini et al., 2009). In this study, we show that the previously uncharacterized TrxG family gene *SDG2* (also named *ATXR3*) plays crucial roles in both sporophyte and gametophyte development.

As in other angiosperms, the *Arabidopsis* life cycle alternates between a prominent diploid sporophytic generation and a much-reduced haploid gametophytic generation. The gametophytic generation occurs late in development within sporophytic tissues of specialized floral organs. Female gametophytes, or megagametophytes, develop in ovules within the gynoecium of the flower (reviewed in Yang et al., 2010). A single megaspore mother cell (megasporeocyte) differentiates from the subepidermal cell layer at the tip of each ovule primordium and undergoes meiosis to produce a tetrad of four haploid spores. Three of the spores degenerate, and one proceeds through three sequential rounds of mitotic division, forming the female gametophyte, the embryo sac, which at maturation consists of seven cells with four cell types (three antipodal cells, two synergid cells, one egg cell, and one two-haploid-fused diploid central cell). The male gametophytes, or microgametophytes, develop within the anthers of the flower (reviewed in Ma, 2005). Microsporocytes differentiate from the primary sporogenous tissue surrounded by the tapetum and undergo meiosis to form a tetrad of four haploid microspores. Each microspore undergoes one cycle of nuclear division, forming a generative cell and a vegetative cell. The generative cell undergoes one more round of mitosis to produce two sperm cells. At maturation, the male gametophyte, the pollen grain, is thus composed of a three-celled male germ unit. Therefore, both female and male gametophyte development consist of two phases: sporogenesis, which starts from reproductive organ differentiation and ends after meiosis by haploid spore formation; and gametogenesis, which consists of haploid cell activities leading to the formation of mature (functional) gametes. The highly coordinated processes of cell division, differentiation, and expansion that take place during female and male gametophyte development require precise fine-tuning of gene regulatory networks.

Transcriptome analyses of male and female gametophytes have provided lists of thousands of differentially expressed genes (Borges et al., 2008; Wuest et al., 2010). In comparison, fewer genes have been functionally characterized in male and/or female gametophyte development (reviewed in Wilson and Zhang, 2009; Yang et al., 2010). The MADS box transcription factor gene *AGAMOUS* (*AG*) specifies reproductive organ identity in flowers (Bowman et al., 1989) and acts in a negative feedback loop to terminate stem cell proliferation in the floral meristem (Lenhard et al., 2001; Lohmann et al., 2001). One of the earliest genes acting downstream of *AG* is *SPOROCTELESS/NOZZLE* (*SPL/NZZ*), which encodes a MADS-like transcription factor (Schieffhale et al., 1999; Yang et al., 1999). The *AG* protein binds the *CARG*-box-like sequence within the 3'-untranslated region of *SPL/NZZ* and activates *SPL/NZZ* expression (Ito et al., 2004). *SPL/NZZ* promotes differentiation of microsporocytes and anther wall cells in the stamens and is necessary for proximal-distal pattern formation, cell proliferation, and early sporogenesis in ovule development (Schieffhale et al., 1999; Yang et al., 1999; Balasubramanian and Schneitz, 2000, 2002;

Sieber et al., 2004). Ectopic expression of *SPL/NZZ* produces hyponastic leaves, defective shoot apical meristems, and abnormal floral organs (Li et al., 2008; Liu et al., 2009). Although direct targets of *SPL/NZZ* have not (yet) been identified, several genes are known to act temporally downstream during gametophyte development. The receptor-like protein kinase gene *EXCESS MICROSPOROCTES1 (EMS1)/EXTRASPOROGENOUS CELL* and the small protein gene *TAPETUM DETERMINANT1 (TPD1)* are required for specifying tapetum and microsporocyte identity (Canales et al., 2002; Zhao et al., 2002; Yang et al., 2003). The bHLH transcription factor gene *DYSFUNCTIONAL TAPETUM1 (DYT1)* and the PHD domain transcription factor gene *MALE STERILITY1 (MS1)* are required for tapetum and microgametophyte development during and after meiosis, respectively (Zhang et al., 2006; Ito et al., 2007; Yang et al., 2007). Reverse genetic analysis revealed that *BTB AND TAZ DOMAIN1 (BT1)* to *BT5* genes have functional redundancy and are essential for female and male gametophyte development (Robert et al., 2009). Large-scale screens of *Ds* transposon insertion lines have identified 67 male and 130 female gametophytic mutants (Pagnussat et al., 2005; Boavida et al., 2009). Among the identified mutant genes, the putative transcription factor genes *EMBRYO SAC DEVELOPMENT ARREST31 (EDA31)* and *MATERNAL EFFECT EMBRYO ARREST65 (MEE65)* are specifically involved in female gametogenesis and gametophyte function, whereas the exostosin-like gene *EDA5* is required for early megagametogenesis as well as for pollen tube growth (Pagnussat et al., 2005; Boavida et al., 2009). Despite the above-described advances, the molecular mechanisms controlling gene transcription within these regulatory networks remain elusive, preventing a deeper understanding of gametophyte pattern formation.

Here, we demonstrate that *sdg2* mutants exhibit both sporophytic and gametophytic development defects. *SDG2* is required for activation of expression of at least 11 genes previously characterized as being essential for gametophyte development. We show that *SDG2* is involved in H3K4me3 deposition at chromatin of some examined genes, including *SPL/NZZ*, *MS1*, and *BT3*. Both *SPL/NZZ* and *MS1* contain bivalent chromatin domains enriched simultaneously with the transcriptionally active mark H3K4me3 and the transcriptionally repressive mark H3K27me3. We propose that *SDG2*-mediated H3K4me3 deposition counteracts H3K27me3-mediated repression of *SPL/NZZ* and *MS1*, forming an important regulatory mechanism in the gene networks underlying gametophyte development.

RESULTS

Identification of Loss-of-Function Mutants of *SDG2*

The *SDG2* gene is predicted to be >10 kb in length, containing 20 introns and 20 exons (Figure 1A). It encodes a putative 2335-amino acid protein containing a SET domain and is predicted at low confidence levels to contain a POST_SET, a GYF, and a NEBULIN domain (Figure 1A). To investigate the biological function of *SDG2*, we obtained six *Arabidopsis* lines, named hereinafter *sdg2-1* to *sdg2-6*, each containing an independent transposon or T-DNA insertion within the *SDG2* locus (Figure 1A).



Figure 1. *SDG2* Gene Structure, Protein Domains, and Phenotype of Loss-of-Function Mutant Alleles.

(A) Exon-intron structure of the *SDG2* gene and domain organization of the predicted *SDG2* protein. Each triangle indicates T-DNA or transposon insertion site in different mutant alleles: 1, *sdg2-1*; 2, *sdg2-2*; 3, *sdg2-3*; 4, *sdg2-4*; 5, *sdg2-5*; and 6, *sdg2-6*. Different protein domains are as follows: a, NEBULIN domain; b, GYF domain; c, SET domain; d, POST_SET domain. aa, amino acids; UTR, untranslated region.

(B) Phenotype comparison of 9-week-old plants between the wild-type *Col* and different allelic *sdg2* mutants. Bars = 2 cm.

(C) Comparison of flower development between *sdg2-1* and *Col*. Some sepals and petals have been removed to expose the inner whorl organs. Numbers indicate flower developmental stages according to Smyth et al. (1990). Note that *sdg2-1* stamens are shorter than *Col* stamens. Bars = 1 mm.

(D) RT-PCR analysis of *SDG2* expression in various *Col* plant organs and in *Col* and *sdg2* mutant seedlings. *ACTIN* serves as an internal control.

All mutations in these lines are recessive; homozygous, but not heterozygous, plants showed an obvious mutant phenotype, which was largely similar across these allelic mutants (Figure 1B). Homozygous mutant plants were smaller in size and were fully sterile (Figures 1B and 1C). RT-PCR analysis revealed that the transposon or T-DNA insertion effectively interrupted production of full-length *SDG2* transcripts in these mutants (Figure 1D).

Taken together, these observations establish that loss of function of *SDG2* causes the phenotype in *sdg2* mutants.

Loss of Function of *SDG2* Results in Smaller Plants

All six allelic *sdg2* mutants have a similar phenotype; we hereafter concentrated on *sdg2-1* for detailed characterization. At the

vegetative stage, *sdg2-1* showed a normal rate of rosette leaf initiation and has similar numbers of rosette leaves at bolting compared with wild-type Columbia (Col) plants (Figure 2A). Also, both *sdg2-1* and Col plants bolted at roughly the same time after sowing. Therefore, differing from the previously characterized TrxG family *Arabidopsis* mutants (Soppe et al., 1999; Kim et al., 2005; Zhao et al., 2005; Pien et al., 2008; Saleh et al., 2008; Xu et al., 2008; Berr et al., 2009; Tamada et al., 2009), *sdg2-1* exhibits a relatively normal flowering time under long-day photoperiod growth conditions. At later developmental stages (after bolting), *sdg2-1* produced fewer secondary rosette leaves compared with Col (Figure 2A). The *sdg2-1* rosette leaves are smaller in size compared with those of Col (Figure 2B). Fresh weight measurements of whole rosettes of 4-week-old plants further confirmed the smaller size of *sdg2-1* (22.0 ± 8.7 mg, $n = 6$)

compared with Col (60.0 ± 12.8 mg, $n = 6$). Light microscopy revealed smaller cell size in *sdg2-1* compared with Col leaves (Figure 2C). The epidermal pavement cell surface is reduced to $\sim 40\%$ in *sdg2-1* compared with Col leaves (Figure 2D). Taken together, these data indicate that cell expansion is drastically constrained, which might largely account for the reduced leaf size in *sdg2-1*. To investigate cell cycle progression, we compared the ploidy levels of *sdg2-1* and Col leaves by measurement of the relative nuclear DNA content via flow cytometry analysis. The 2C and 4C DNA content corresponds to the G1 and G2 phases during mitotic division, respectively. The proportion of 2C cells is slightly lower in *sdg2-1* compared with Col (Figure 2E), suggesting a relatively shorter duration of G1 in the mutant. Higher ploidy levels ($\geq 8C$) are the result of endoreduplication cycles in which nuclear DNA is replicated without a subsequent

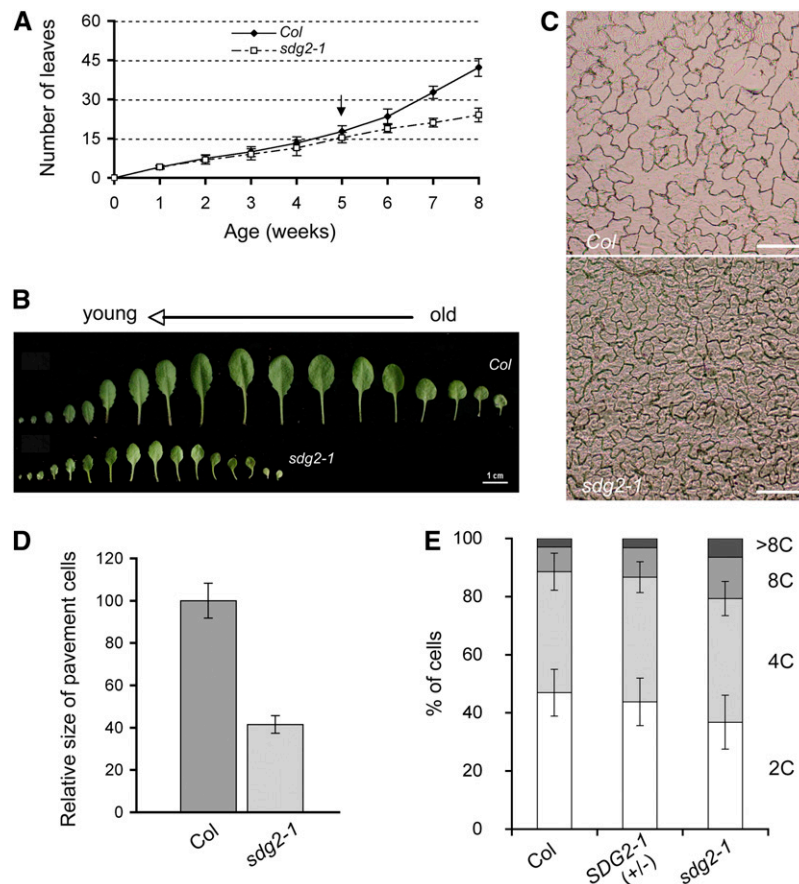


Figure 2. Comparison of Leaf Initiation and Phenotype between the *sdg2-1* Mutant and Wild-Type Col.

(A) Leaf initiation evaluated by total number of leaves per plant over the time course of plant growth. Mean values from 10 plants are shown, and error bars indicate SD. Arrow indicates age point from which plants start flowering.

(B) True leaves dissected from individual plants at 6 weeks old. Bar = 1 cm.

(C) Differential interference contrast (DIC) images of mature leaf adaxial epidermal cells from the seventh true leaf of 6-week-old plants. Bars = 100 μ m.

(D) Relative size of leaf adaxial epidermal pavement cells evaluated by measurement of the cell area from DIC images. The y axis indicates the relative cell size (wild type is set to 100%) calculated from the mean value of 30 cells, and error bars indicate SD.

(E) Ploidy levels of cells from leaves of 2-week-old plants. Mean values from two independent experiments are shown. Error bars indicate SD. *SDG2-1 (+/-)* depicts heterozygous plants of the mutant.

[See online article for color version of this figure.]

mitotic division. The relative proportion of cells with higher ploidy levels is slightly increased in *sdg2-1* compared with Col (Figure 2E); moreover, cycle value, defined as the mean number of endoreduplication cycles per nucleus (Barow and Meister, 2003), is significantly ($P < 0.001$) higher in *sdg2-1* (0.857 ± 0.083 , $n = 10,000$) than in Col (0.614 ± 0.228 , $n = 10,000$). These latter results indicate that mutant cells exit the mitotic cycle and undergo cell differentiation earlier.

Anther and Pollen Development Is Impaired in *sdg2-1* Mutant Plants

The most remarkable phenotype of the *sdg2* mutant plants is their sterility. *Arabidopsis* floral organs are arranged in four concentric whorls, from the outermost to the innermost: the sepals, petals, stamens, and pistil. *sdg2* mutant flowers contain normal numbers of floral organs and a relatively normal morphology, except that the stamens remain short during later flower developmental stages (stage definition according to Smyth et al., 1990; Figure 1C). Homeotic conversion of floral organs, as had been previously reported for the *atx1-1* (Alvarez-Venegas et al., 2003) and *sdg8-1/ashh2-1* (Grini et al., 2009) mutants, was not observed in *sdg2* mutants. In *sdg2* mutants, the short stamens failed to reach the receptive stigmatic papillae of the pistil at anthesis for successful pollination. In addition, pollen production is also affected. Cytological analysis revealed aberrant anthers in *sdg2-1* that lack one or more of the four locules (Figure 3A; see Supplemental Figure 1 online), indicating defects in initiation, specification, and/or development of primary sporogenous and tapetal cells in the mutant. In some locules, sporogenous cells developed and produced pollen grains; however, these pollen grains stuck to each other and anther dehiscence failed to occur efficiently. Over 40% of pollen grains showed collapsed morphology (Figures 3B and 3C), and Alexander staining revealed both viable and dead pollen grains in *sdg2-1* locules (Figure 3D). Compared with Col pollen, viable *sdg2-1* pollen was larger in size, and organization of the male germ unit showed irregular positioning of the two sperm and single vegetative cell nuclei (Figure 3E). To test whether viable *sdg2-1* pollen is functional, we gently dissected pollen grains from mature anthers and used them to pollinate pistils of emasculated Col plants. From 24 pollinated pistils (containing a total of ~ 1200 ovules), we obtained 45 seeds, which were confirmed by PCR analysis to correspond to the expected heterozygous mutant genotype. The very low fertilization efficiency indicates that only a very small number of *sdg2-1* pollen grains are fully functional.

SDG2 Is Necessary for Male Gametogenesis

The *sdg2-1* pollen phenotype and functional defects indicate that SDG2 is required for proper microgametogenesis. To gain further information, we examined tetrads dissected from *sdg2-1* and Col immature anthers by 4',6-diamino-2-phenylindole (DAPI) staining. Col tetrads contained the expected four haploid microspores, with four DAPI-stained nuclei visible (Figure 3F), whereas the *sdg2-1* tetrads showed a variable reduced number of nuclei (Figure 3G). Quantitative analysis revealed that whereas $>97\%$ of Col tetrads contain the normal four DAPI-stained nuclei, only

$\sim 50\%$ of *sdg2-1* tetrads show such configuration and the remaining 50% of tetrads contain lower numbers of nuclei (Figure 3H). Abnormal *sdg2-1* tetrads are also visible inside the pollen sac upon cytological examination (Figure 3I). Light microscopy images of *sdg2-1* tetrads showed that microspores without DAPI staining are surrounded by a cell wall, suggesting that cytokinesis occurs relatively normally during cell division. The absence of DAPI staining and some aberrant DAPI-staining structures (Figure 3G) suggest that abnormal chromatin organization, nucleus degeneration, and DNA degradation had occurred during *sdg2-1* microspore formation.

To examine gametophyte function under normal sporophytic growth, we investigated inheritance of *sdg2* mutant alleles in heterozygous mutant plants. The *sdg2-1* allele is associated with an insertion transgene expressing phosphinothricin resistance. Growth tests on seeds produced by self-pollination of heterozygous *SDG2-1+/-* plants revealed that phosphinothricin-resistant compared with phosphinothricin-sensitive plant numbers are significantly lower than the expected ratio of 3:1 (Table 1). The *SDG2-2+/-* and *SDG2-3+/-* lines behaved very similarly to *SDG2-1+/-* (Table 1). As no seed abortion could be observed, this suggested that male and/or female transmission of the *sdg2* mutant alleles was decreased. To determine the inheritance of the *sdg2* mutant alleles in the male and female gametes, reciprocal backcrosses of heterozygous mutant plants with the wild-type plants were performed. Genotyping by PCR analysis revealed that the inheritance of both the *sdg2-1* and *sdg2-3* alleles was reduced drastically through male and also slightly but significantly through female gametes (Table 1). Together, these genetic data establish a gametophytic function of SDG2, which is largely independent from its sporophytic function.

Ovule and Female Gametophyte Development Is Defective in *sdg2-1* Mutant Plants

To investigate functionality of female gametophytes in homozygous *sdg2-1* plants, we first examined their fecundity by pollination of mutant pistils with Col pollen grains. From a total of 90 pistils from 10 *sdg2-1* plants examined in two independent experiments, we failed to obtain any seeds from pollination of *sdg2-1* pistils, indicating that *sdg2-1* is completely female sterile. We used light microscopy to examine ovule development. It is well known that in wild-type *Arabidopsis* plants, ovule development is synchronous and follows several distinct stages (Christensen et al., 1997). We observed that early-stage premeiotic ovules contain single megaspore mother cells in *sdg2-1* as in Col (Figures 4A and 4B). After meiosis, the three spores closest to the micropyle of the ovule undergo programmed cell death and the chalazal megaspore undergoes mitosis to give rise to a two-nucleate embryo sac, as observed for Col (Figure 4C). However, most *sdg2-1* ovules are defective, showing obvious abnormalities in megaspores and the development of the embryo sac (Figures 4D and 4E). Some *sdg2-1* ovules show overproliferation of the nucellus at the tip (Figure 4D). We further analyzed embryo sac formation using confocal laser scanning microscopy. In Col ovules, the embryo sac at maturation is well surrounded by integument tissues and consists of one egg cell, one central cell, two synergid cells, and at the chalazal pole, three antipodal cells

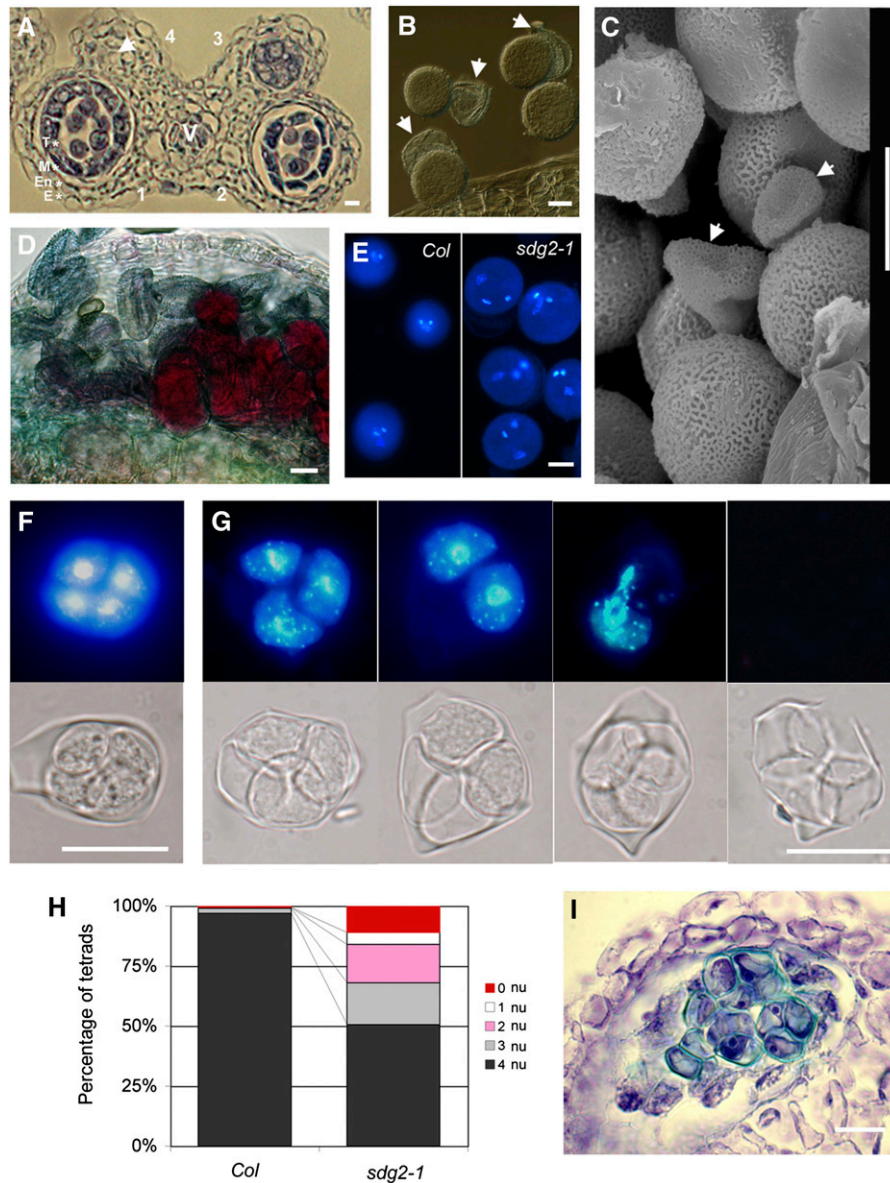


Figure 3. *sdg2-1* Exhibits Wide-Ranging Defects in Anther and Male Gametophyte Development.

(A) Transverse section of *sdg2-1* anther. *Arabidopsis* anthers consist of four locules (numbered on the micrograph). A normal locule, as indicated for locule 1, consists of microsporocytes surrounded by four nonreproductive cell layers, from the interior to the surface: the tapetum (T), the middle layer (M), the endothecium (En), and the epidermis (E). As indicated by the arrow, locule 4 is developmentally arrested, and microsporocytes and the tapetal layer are absent. V indicates vasculature.

(B) *sdg2-1* pollen grains at anthesis. Arrows indicate collapsed pollen grains.

(C) Scanning electron micrograph of *sdg2-1* pollen grains. Arrows indicate collapsed pollen grains.

(D) Alexander staining of pollen grains within an *sdg2-1* locule. Defective pollen is light green, and viable pollen is dark red or pink.

(E) Comparison between Col and *sdg2-1* DAPI-stained pollen. Each pollen grain contains two densely stained sperm cell nuclei and one larger/more diffuse vegetative cell nucleus.

(F) and **(G)** Col and *sdg2-1* tetrad phenotypes, respectively. Top panels show DAPI staining, and bottom panels show corresponding DIC images. Representative images of different mutant phenotypes are shown for *sdg2-1*.

(H) Quantitative analysis of tetrad phenotypes. Percentage of tetrads showing variable number of DAPI-stained nuclei (nu) was calculated from a total of 200 tetrads each for Col and *sdg2-1*.

(I) Transverse section through an *sdg2-1* locule showing presence of abnormal tetrads inside.

Bars = 10 μ m for **(A)** to **(G)** and **(I)**.

Table 1. Segregation Analysis of *sdg2* Mutant Alleles in Progeny Derived from Self-Pollination or Crosses

| Parent | Progeny ^{a,b} | | Observed Ratio ^c | Expected Ratio |
|--------------------------------|------------------------|------|-----------------------------|----------------|
| Self-Pollination | S | R | S:R | S:R |
| <i>SDG2-1+/-</i> selfing | 657 | 1099 | 1:1.67*** | 1:3 |
| <i>SDG2-2+/-</i> selfing | 2093 | 4756 | 1:2.27*** | 1:3 |
| <i>SDG2-3+/-</i> selfing | 1337 | 2738 | 1:2.05*** | 1:3 |
| Crosses | SS | Ss | SS:Ss | SS:Ss |
| Col (♀) × <i>SDG2-1+/-</i> (♂) | 74 | 43 | 1:0.58** | 1:1 |
| Col (♀) × <i>SDG2-3+/-</i> (♂) | 62 | 34 | 1:0.55** | 1:1 |
| <i>SDG2-1+/-</i> (♀) × Col (♂) | 158 | 130 | 1:0.82 ⁻ | 1:1 |
| <i>SDG2-3+/-</i> (♀) × Col (♂) | 161 | 127 | 1:0.79* | 1:1 |

^aAlleles of *sdg2-1*, *sdg2-2*, and *sdg2-3* are associated with phosphinothricin, sulfadiazine, and kanamycin resistance marker genes. Numbers of sensitive (S) and resistant (R) plants grown on selective media are used to investigate transmission of mutant alleles.

^bWild-type *SDG2* (S) and mutant *sdg2* (s) alleles were determined by PCR analysis. Numbers of plants with Col (SS) and *SDG2-1+/-* or *SDG2-3+/-* (Ss) genotypes are shown.

^cThe ratios obtained from experimental data are lower than those expected from normal segregation, indicating reduced transmission efficiency of mutant alleles. Statistical significance: ***P < 0.001; **P < 0.01; *P < 0.05; ⁻P > 0.05.

undergoing cell death (Figure 4F). *sdg2-1* ovules showed abnormal phenotypes and could essentially be divided into three different classes. The first class, which accounted for ~56% of all ovules, showed relatively normal integument development and nucellus proliferation but did not contain an obvious embryo sac (Figure 4G). The second class represented ~28% of all ovules and showed inhibition of integument growth and nucellus overproliferation at the tip and also lacked an obvious embryo sac (Figure 4H). In these two classes, arrest of embryo sac development might occur before vacuole formation, which normally takes place at the two-nucleate stage. No clear nuclear morphology could be observed and some staining structures revealed cell death (Figures 4G and 4H), indicating that in both classes, megaspores are degenerated during early gametophyte development. Finally, the third class, accounting for ~16% of all ovules, contained a vacuolated embryo sac but displayed degeneration of nuclei and cell death prior to embryo sac maturation (Figure 4I). Taken together, our observations indicate that *SDG2* plays crucial roles at various stages of ovule and female gametophyte development. The fact that *SDG2* functions in megagametogenesis is also demonstrated by the reduced inheritance of mutant alleles in the heterozygous *SDG2-3+/-* and *SDG2-1+/-* plants (Table 1).

***SDG2* Transcripts Are Detected at High Levels in Sporogenous/Gametophytic Cells in Anthers and Ovules**

SDG2 expression in Col plants was detected by RT-PCR in various tissue types, with the highest level observed in flower buds (Figure 1D). We further investigated *SDG2* expression by in situ hybridization. We detected *SDG2* transcripts at high levels in primordia and young floral organs (Figure 5A). At later stages, high levels of *SDG2* transcripts were observed in sporogenous cells and microsporocytes in anther locules (Figure 5B). For comparison, *AG* transcripts were detected specifically in reproductive organ primordia and in anther cells prior to microsporocyte formation (Figure 5C), as previously reported (Bowman et al., 1991; Ito et al., 2004); and *SPL/INZZ* transcripts were

detected in floral organ primordia, in tapetal and sporogenous cells as well as in microspores (Figure 5D), as previously reported (Schiefthaler et al., 1999; Yang et al., 1999). *SDG2* transcripts were also detected in ovules within the pistil (Figure 5E) and in the embryo sac (Figure 5F). *SDG2* transcripts were present at low levels in young embryos before the heart stage (Figure 5G) but were undetectable in mature embryos (Figure 5H). As expected, *SDG2* transcripts were not detected in *sdg2-1* flowers at all stages examined (shown for ovules in Figure 5I). As a negative control, hybridization with an *SDG2* sense gene probe did not reveal detectable signals in Col or *sdg2-1* in all tissues tested (data not shown). The observed *SDG2* expression pattern in anthers and ovules is consistent with its proposed function during male and female gametophyte development.

Genes Essential for Gametophyte Development Are Downregulated in *sdg2-1* Flower Buds

To investigate the molecular mechanisms underlying the observed defects in *sdg2-1* gametophyte development, we analyzed transcript profiles in the *sdg2-1* mutant by microarray analysis (Agilent Technologies). We compared *sdg2-1* and Col transcripts obtained from young flower buds around stage 8 of flower development (Smyth et al., 1990). At this stage, locules begin to appear in stamens, and ovule primordia are detectable as interdigitating finger-like protrusions in the pistil. This flower developmental stage was chosen to avoid the severe developmental defects that occur later during gametogenesis in the *sdg2-1* mutant. We found 452 genes downregulated (see Supplemental Data Set 1A online) and 273 genes upregulated (see Supplemental Data Set 1B online) by more than twofold in *sdg2-1* floral buds compared with Col.

Remarkably, 11 genes previously shown to be essential for gametophyte development were among the downregulated genes in *sdg2-1* (Table 2). We further investigated the expression of several genes essential for gametophyte development by quantitative RT-PCR analyses. These included seven genes, *SPL/INZZ*, *BT3*, *DYT1*, *MS1*, *MYB99*, *EDA31*, and *MEE65* (listed

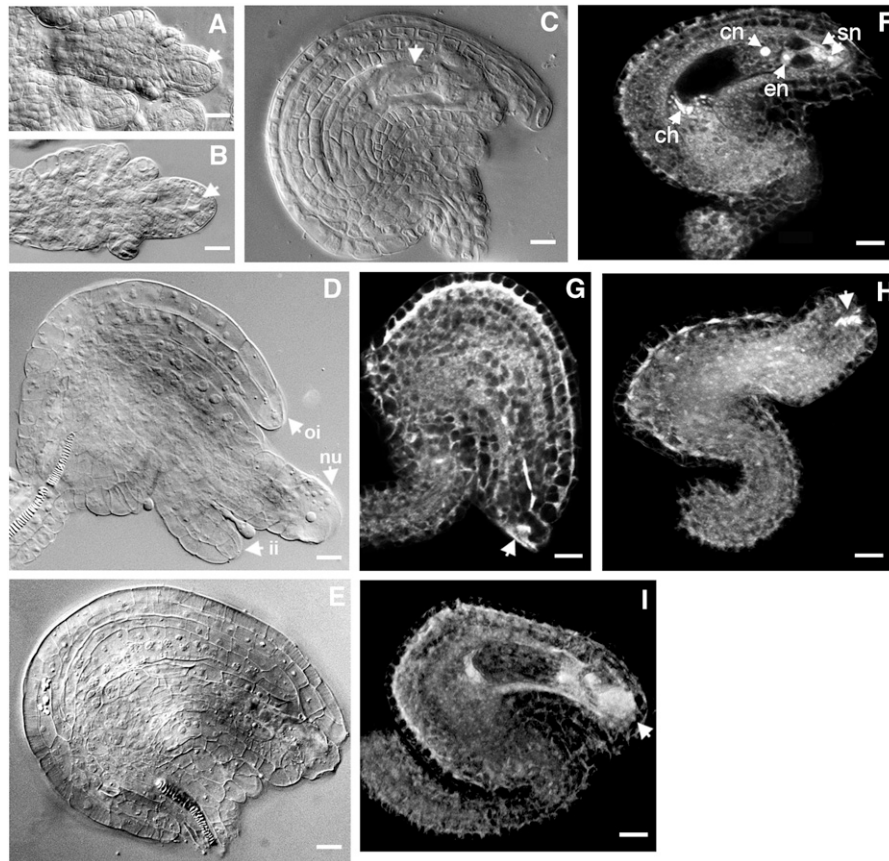


Figure 4. *sdg2-1* Shows Severe Defects in Ovule and Female Gametophyte Development.

(A) and (B) DIC images of ovule primordia in Col and *sdg2-1*, respectively. Arrows indicate archesporial/megasporogenous cells.

(C) to (E) DIC images of a Col ovule at the two-nucleate embryo sac stage (C) and of *sdg2-1* ovules at later developmental stages (D) and (E). Note the absence of an obvious embryo sac and the disproportionate nucellus and integument proliferation in *sdg2-1* ovules. Arrows indicate a two-nucleate embryo sac in Col (C) and abnormal nucellus (nu), inner integument (ii), and outer integument (oi) in *sdg2-1* (D).

(F) to (I) Three-dimensional reconstruction images of confocal sections of Col (F) and *sdg2-1* (G) to (I) mature ovules. In the Col ovule, arrows indicate the following: ch, chalazal region containing three degenerating antipodal cell nuclei; cn, diploid central cell nucleus; en, egg cell nucleus; and sn, two synergic cell nuclei at the micropylar end. In *sdg2-1* ovules, arrows indicate the micropylar end with signs of degenerating cells visible as brightly fluorescent abnormal structures.

Bars = 10 μ m.

in Table 2), together with *EMS1* and *TPD1*, which were not among the list of differentially expressed genes identified in *sdg2-1* by microarray analysis but were previously shown to act early in the determination of tapetal cell identity (Canales et al., 2002; Zhao et al., 2002; Yang et al., 2003). Consistent with transcriptome analysis data, RT-PCR analysis showed that expression of *SPL/NZZ*, *BT3*, *DYT1*, *MS1*, *MYB99*, *EDA31*, and *MEE65* was downregulated, whereas expression of *EMS1* and *TPD1* was unchanged in *sdg2-1* flower buds compared with Col (Figure 6).

Among the identified genes, *BT3* is involved in both male and female gametophyte development (Robert et al., 2009). Nevertheless, because the *bt3* mutant displays a wild-type phenotype and only the double mutant *bt2 bt3* shows defects in gametophyte development (Robert et al., 2009), we believe that downregulation of *BT3* alone, as identified in the *sdg2-1* mutant, has

little effect on the *sdg2-1* mutant phenotype. *SPL/NZZ* is unique in that it is required early in both male and female gametophyte development (Schiefthaler et al., 1999; Yang et al., 1999). The other nine genes are known to be involved downstream of *SPL/NZZ* and at later developmental stages in either male or female gametophyte development (Table 2). Some of the early gametophyte developmental defects observed in *sdg2-1* partially phenocopy the *spl/nzz* mutant. In addition, both *SPL/NZZ* and *SDG2* expression can be found in sporogenous cells and microsporocytes in anthers and in megasporocytes in ovules (Schiefthaler et al., 1999; Yang et al., 1999; Figure 5). To examine expression differences in a tissue-specific manner, we compared *SPL/NZZ* expression in *sdg2-1* and in Col by in situ hybridization. As shown in Figure 7, *SPL/NZZ* expression is clearly reduced in ovule primordia and in sporogenous cells and microsporocytes within anthers in *sdg2-1* compared with Col. This is consistent

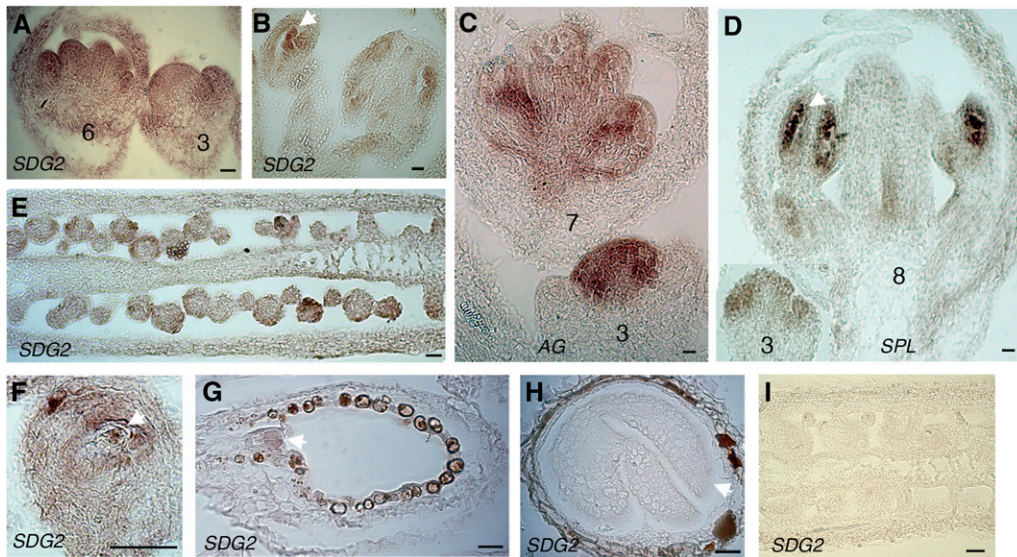


Figure 5. In Situ Hybridization Analysis of *SDG2* Expression.

- (A) Longitudinal section through two *Col* flower buds at developmental stages 3 and 6, probed for *SDG2*.
 (B) Longitudinal section through *Col* anthers at flower developmental stage 8, probed for *SDG2*. Arrow indicates microsporocyte surrounded by tapetum within a locule.
 (C) Longitudinal section through two *Col* flower buds at developmental stages 3 and 7, probed for *AG*.
 (D) Longitudinal section through two *Col* flower buds at developmental stages 3 and 8, probed for *SPL*. Arrow indicates microsporocyte within a locule.
 (E) Longitudinal section through part of a *Col* gynoecium at flower developmental stage 11-12, probed for *SDG2*.
 (F) Longitudinal section through *Col* ovule, probed for *SDG2*. Arrow indicates the embryo sac.
 (G) and (H) Longitudinal sections through *Col* seeds at quadrant and bent-cotyledon embryo stages, respectively, probed for *SDG2*. Arrow indicates embryo.
 (I) Longitudinal section through part of an *sdg2-1* gynoecium at flower developmental stage 11-12, probed for *SDG2*.

Hybridization signals are dark-brown/pink areas. Negative controls using a sense probe did not generate detectable signal. Note that endothelial cells surrounding the embryo are frequently colored, which resembles the hybridization signal. This occurs without application of probe and is caused by plant metabolites. Bars = 10 μm .

with transcriptome (Table 2) and RT-PCR (Figure 6) analysis data.

***SDG2* Activates Gene Transcription through H3K4 Trimethylation**

To gain insight into the molecular mechanism of *SDG2*-mediated activation of gene expression, we investigated histone methylation levels in *sdg2-1*. Protein immunoblot analysis (Figure 8A) showed that compared with *Col*, *sdg2-1* plants contain a dramatically reduced level of H3K4me₃, a slightly reduced level of H3K4me₂, and an enhanced level of H3K4me₁. By contrast, levels of H3K36me₁, H3K36me₃, and H3K27me₃ were unchanged in *sdg2-1* compared with *Col* (Figure 8A). This indicates that *SDG2* is required primarily for H3K4me₃ deposition and, to a lesser degree, H3K4me₂ deposition in *Arabidopsis*. H3K4me₁ deposition likely involves a different enzyme, and defects in converting monomethyl to di-/trimethyl by *sdg2-1* might have elevated H3K4me₁ levels as observed in the *sdg2-1* mutant plants.

We further investigated H3K4me₃ and H3K27me₃ at specific genes by chromatin immunoprecipitation (ChIP) assays (Figures 8B and 8C). H3K4me₃ levels were drastically reduced at *BT3* and *SPL/NZZ* in *sdg2-1* compared with *Col*. Compared with *BT3* or *SPL/*

NZZ, *MS1* contains lower levels of H3K4me₃ in *Col*. Nevertheless, significant ($P < 0.01$) reductions in H3K4me₃ were also observed at *MS1* in the *sdg2-1* mutant compared with *Col*. By contrast, *EDA31* and *MEE65* contain low levels of H3K4me₃ that are barely affected in *sdg2-1*. At all examined genes, levels of H3K27me₃ were not significantly different in *sdg2-1* compared with *Col*.

Interestingly, relatively high levels of both H3K4me₃ and H3K27me₃ were detected at *SPL/NZZ* and *MS1* in *Col* plants. To investigate whether H3K4me₃ and H3K27me₃ simultaneously mark *SPL/NZZ* and *MS1* chromatin or if they are derived from subpopulations of cells exhibiting different chromatin configurations, we performed sequential double ChIP analysis. Chromatin was immunoprecipitated first with anti-H3K27me₃ and then with anti-H3K4me₃ antibodies. The results obtained are shown in Figure 8D. Consistent with previously reported data (Jiang et al., 2008), we found that chromatin at both *FLOWERING LOCUS T (FT)* and *FLOWERING LOCUS C (FLC)* concomitantly carries both H3K27me₃ and H3K4me₃, whereas *ACTIN2 (ACT2)* chromatin does not. Like *FT* and *FLC*, *SPL/NZZ* and *MS1* chromatin also simultaneously carry both H3K27me₃ and H3K4me₃ marks. Reduced levels in *sdg2-1* were observed specifically at *SPL/NZZ* and *MS1* loci but not at *FT* and *FLC* (Figure 8D).

Table 2. Downregulated Genes in *sdg2-1* That Are Known to Be Functionally Essential for Gametophyte Development

| Probe Name | P Value | Fold Change | Gene ID | Gene Symbol | Description | Reference |
|--------------|---------|-------------|-----------|--------------------------------|--|--|
| A_84_P20471 | 0.001 | 2.1 | At4g27330 | <i>SPL/NZZ</i> | Male and Female Gametophyte Development SPOROCTELESS/NOZZLE; a putative MADS-like transcription factor | Schieffhaller et al. (1999); Yang et al. (1999) |
| A_84_P832776 | 0.017 | 2.1 | At1g05690 | <i>BT3</i> | BTB and TAZ domain protein 3; a putative transcription regulator | Robert et al. (2009) |
| A_84_P14769 | 0.011 | 2.2 | At4g21330 | <i>DYT1</i> | Male Gametophyte Development DYSFUNCTIONAL TAPETUM1; a putative bHLH domain transcription factor | Zhang et al. (2006) |
| A_84_P15962 | 0.010 | 2.6 | AT5G56110 | <i>MYB80</i> <i>/MYB103</i> | MYB DOMAIN PROTEIN 80/103; a putative transcription factor | Zhang et al. (2007) |
| A_84_P565469 | 0.047 | 2.8 | At5g22260 | <i>MS1</i> | MALE STERILITY1; a putative PHD domain transcription factor | Ito et al. (2007); Yang et al. (2007) |
| A_84_P12806 | 0.039 | 2.8 | At3g60460 | <i>DUO1</i> | DUO POLLEN1; a putative myb family transcription factor | Rotman et al. (2005) |
| A_84_P13673 | 0.018 | 3.1 | At3g11980 | <i>MS2</i> | MALE STERILITY2; fatty acid reductase | Aarts et al. (1997) |
| A_84_P14098 | 0.016 | 3.9 | At5g62320 | <i>MYB99</i> | Myb domain protein 99; a putative transcription factor | Alves-Ferreira et al. (2007) |
| A_84_P15477 | 0.012 | 2.5 | At3g10000 | <i>EDA31</i> | Female Gametophyte Development EMBRYO SAC DEVELOPMENT ARREST31; SANT, MYB-like transcription factor | Pagnussat et al. (2005) |
| A_84_P78785 | 0.012 | 2.9 | At3g03650 | <i>EDA5</i> | EMBRYO SAC DEVELOPMENT ARREST5; exostosin-like | Pagnussat et al. (2005) |
| A_84_P579221 | 0.039 | 8.2 | At2g01280 | <i>MEE65</i> | MATERNAL EFFECT EMBRYO ARREST65; transcription factor TFIIB-related | Pagnussat et al. (2005) |

Taken together, our ChIP data show that *SDG2* mediates H3K4me3 deposition selectively at *BT3*, *SPL/NZZ*, and *MS1*, which is consistent with the transcriptional repression of these genes in *sdg2-1*. H3K4me3 levels in *sdg2-1* were unchanged at *FLC* and *FT*, which is in agreement with unchanged expression of these genes and the unchanged flowering time phenotype of the mutant. *EDA31* and *MEE65* do not show detectable changes in H3K4me3, suggesting that their reduced expression could be a secondary effect in the *sdg2-1* mutant. Our results also reveal that *SPL/NZZ* and *MS1* are embedded in bivalent chromatin domains, which simultaneously contain the transcriptionally active mark H3K4me3 and the transcriptionally repressive mark H3K27me3.

DISCUSSION

Over two-thirds of all *Arabidopsis* nuclear genes contain chromatin marked by H3K4 methylation (Zhang et al., 2009). Among previously characterized TrxG family mutants, only *atx1* showed a mild reduction in the global level of H3K4me3 (Alvarez-Venegas and Avramova, 2005). Gene locus-specific reduction of H3K4 methylation was observed in *atx1* (Alvarez-Venegas and Avramova, 2005; Pien et al., 2008), and also in *atx2* (Saleh et al., 2008) and *sdg25/atxr7* (Tamada et al., 2009). Our study establishes that *SDG2* is a major factor for H3K4me3 deposition in *Arabidopsis*. *sdg2-1* showed a global reduction of H3K4me3 in total histone extracts (Figure 8), which is more pronounced than that observed in *atx1* (see Supplemental Figure 2 online). Consistent with this,

SDG2 has a broad function, and *sdg2* mutants show pleiotropic phenotypes.

SDG2 in Regulation of Sporophyte Development

The *sdg2* mutant plants are small in size, which is visible across a variety of organs, including leaves, stems, and flowers. The previously characterized *atx1-1* and *sdg8/efs/ccr1* mutants also exhibit reduced plant and organ sizes (Soppe et al., 1999; Alvarez-Venegas et al., 2003; Xu et al., 2008). These data thus reveal that global levels of H3K4me3 and H3K36me2/3 have an overall positive role in plant growth. Plant size is intrinsically determined by cell division and cell expansion activities. The initiation of a leaf begins with the periclinal division of a cell in the L2 layer of the shoot apical meristem, which grows out into the leaf primordium and then forms the mature leaf. In contrast with the indeterminate growth of apical meristems, leaves show determinate growth with a fixed period of development. Our investigation shows that leaf initiation is relatively normal during vegetative growth in *sdg2-1*; however, final leaf size is drastically reduced in *sdg2-1* compared with Col. The reduced leaf size is largely associated with a major reduction of cell expansion. Moreover, cell division and differentiation in *sdg2-1* is also affected; the G1 phase is relatively shorter, and polyploidy levels are slightly enhanced in the *sdg2-1* mutant leaves.

Endoreduplication occurs after cells have ceased mitotic cycles, and endoreduplicated cells do not reenter the mitotic cell cycle. Endoreduplication is thus characteristic of a switch between cell proliferation and differentiation. It is also believed to

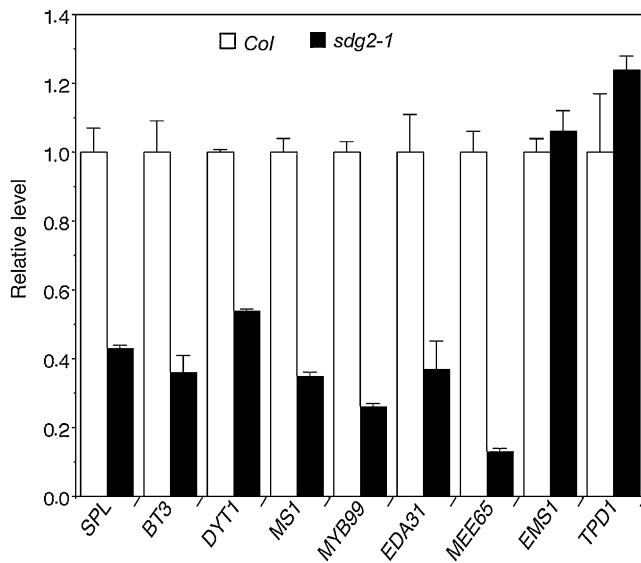


Figure 6. Quantitative RT-PCR Analysis of Gene Expression in Col and *sdg2-1* Flower Buds at Developmental Stage 8.

Relative expression levels are calculated from mean values of three replicates from two independent biological samples. Error bars show SD.

be essential for enhancing metabolic capacity and supporting cell growth and for maintaining an optimal balance between cell volume and nuclear DNA content (reviewed in Kondorosi et al., 2000; Inzé and De Veylder, 2006). Curiously, *sdg2-1* shows slightly elevated polyploidy levels but reduced cell size. Ploidy-dependent epigenetic regulation has been reported to be involved in differential reprogramming of orthologous gene expression and in stable silencing of epialleles (Lee and Chen, 2001; Baubec et al., 2010). Based on its global effect on H3K4me3 deposition, it is reasonable to speculate that *SDG2* is involved in regulation of chromatin structure and gene expression in diploid and polyploid cells, playing important roles in the coordination of cell division, differentiation, and expansion to determinate organ size.

Although *SDG2* transcripts were detectable in the inflorescence meristem and in floral organ primordia, *sdg2* mutant flowers showed the normal order of the four whorls and normal numbers of floral organs. Flower organ identity is determined by the interplay between homeotic transcription factor genes, including *AG*, *PI*, *AP3*, *AP2*, and *AP1*, which are subjected to chromatin-remodeling regulation (reviewed in Shen and Xu, 2009). Consistent with its phenotype, *sdg2-1* did not show any detectable alteration of expression of these floral homeotic transcription factor genes in our microarray analysis. By contrast, downregulation of *AG*, *PI*, *AP2*, and *AP1* was shown in *atx1-1*, with flowers exhibiting homeotic conversions and variable aberrations (Alvarez-Venegas et al., 2003). *sdg8-1/ashh2-1* has also been reported to display downregulation of *PI*, *AP2*, and *AP1*, with a low proportion of flowers exhibiting homeotic conversions (Grini et al., 2009). Furthermore, the *sdg2* mutants differ in the flowering time phenotype from previously studied TrxG family gene mutants. Both activation and repression of *FLC*

depend on chromatin remodeling activities (for recent reviews, see He, 2009; Berr and Shen, 2010), and *sdg8/efs/ashh2*, *sdg25/atx7*, *atx1*, and *atx2* mutants exhibit reduced *FLC* expression associated with a decrease of H3K4me2/me3 and/or H3K36me2/me3 at *FLC* chromatin (Kim et al., 2005; Zhao et al., 2005; Pien et al., 2008; Saleh et al., 2008; Xu et al., 2008; Berr et al., 2009; Tamada et al., 2009). Despite its broad effects, *sdg2-1* did not alter H3K4me3 levels at *FLC*, and the mutant plants showed a wild-type flowering time under long-day photoperiod growth conditions, revealing the selectivity of *SDG2*-dependent H3K4me3 deposition and transcription activation. Overlapping and specific roles of different members within the TrxG family might allow for more flexibility in functions associated with plant growth and developmental plasticity.

***SDG2* in Regulation of Gametophyte Development**

The *sdg2* mutant plants show complete sterility. At least three defects contribute to *sdg2-1* sterility: first, stamen filaments are too short to allow effective pollination of the stigma; second, anther dehiscence and production of functional pollen is drastically impaired; and third, ovules lack a fully developed, functional embryo sac. In *sdg2-1*, anther and pollen development show a variety of defects from early to late stages, including sporophytic locule initiation, microsporogenesis, tapetum development, and microgametogenesis. Late function of viable pollen grains also seems to be affected as indicated by the very low efficiency of seed production obtained using *sdg2-1* pollen in pollination of wild-type pistils. In addition, for >80% of *sdg2-1* ovules, megagametogenesis is arrested before the completion of the mitotic haploid divisions. For <20% of *sdg2-1* ovules, a vacuolated embryo sac is visible, but the megaspore nucleus degenerates before embryo sac maturation. Defects were also observed in sporophytic tissues within *sdg2-1* ovules. High levels of *SDG2* expression were detected in reproductive organs with specific patterns that are consistent with the important role of *SDG2* in gametophyte development. The pleiotropy and variable expressivity of the *sdg2-1* phenotype makes it distinct from transcription factor mutants that display a specific defect in one or a few stages of male or female gametophyte development. The main requirement for *SDG2* is likely in the sporophyte for proper development or function of anthers and ovules and sporogenesis. Nevertheless, *SDG2* also has important roles in gametogenesis as evidenced by late stage defective gametophytes observed in *sdg2-1* and more importantly by the reduced transmission efficiency of mutant alleles in heterozygous mutant plants (Table 1).

Nuclear degeneration and genomic DNA degradation likely occur in both microspore and megaspore cells in *sdg2-1*. We hypothesize that *SDG2*-mediated H3K4me3 deposition plays an important role in chromosomal organization and reprogramming during meiosis. In yeast, H3K4me3 serves as a prominent mark of active meiotic recombination initiation sites, and loss of function of the sole H3K4 methyltransferase SET1 causes reduced formation of DNA double-strand breaks, which are essential for proper chromosome segregation and fertility (Borde et al., 2009). In mammals, germ cell-specific *PRDM9* (also known as *Meisetz*), which is involved in H3K4me3 but not H3K4me2 or

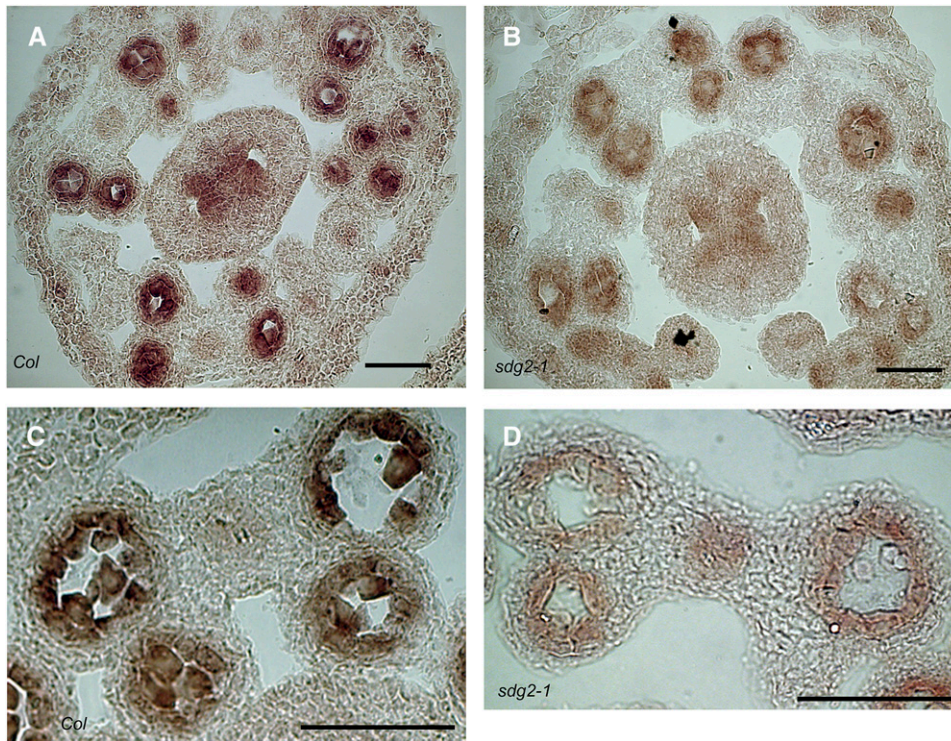


Figure 7. In Situ Hybridization Analysis of *SPL/NZZ* Expression in *Col* and *sdg2-1* Floral Organs.

(A) and (B) Transverse section through flower bud at developmental stage 7-8 in *Col* and *sdg2-1*, respectively. (C) and (D) Transverse section through anther at flower developmental stage 8-9 in *Col* and *sdg2-1*, respectively. Bars = 50 μ m.

H3K4me1 deposition, is necessary to guide recombination hotspots of homologous chromosomes during meiotic prophase (Hayashi et al., 2005; Hochwagen and Marais, 2010). Nevertheless, we currently do not know if meiotic recombination is affected in the *sdg2* mutants. Alternatively, *SDG2* might regulate chromatin structure and function during gamete formation after meiosis. Distinct from yeast and mammals, plant gametogenesis occurs within highly structured sporophytic tissues. Coordination with sporophytic tissue development is essential for proper plant gametogenesis, and *SDG2* plays an important role in the establishment of expression patterns of sporophytic and gametophytic genes.

***SDG2* Positively Regulates H3K4me3 Deposition and Expression of Some Gametophyte Development Genes**

At least 11 genes previously shown to play essential functions in gametophyte development were identified as downregulated in *sdg2-1* flower buds (Table 2). Among them, the MADS-like transcription factor gene *SPL/NZZ* is of particular interest. It acts upstream of many stamen- and ovule-expressed genes and is required for initiation of both microsporogenesis and megasporogenesis (Schiefthaler et al., 1999; Yang et al., 1999; Yu et al., 2005; Zhang et al., 2006; Alves-Ferreira et al., 2007; Wijeratne et al., 2007). Although knowledge is currently scarce about how *SPL/NZZ* regulates downstream processes, a gain-

of-function study suggested that *SPL/NZZ* might be involved in auxin homeostasis by repression of *YUCCA* genes in lateral organ development (Li et al., 2008). The phytohormone auxin was recently shown to have an important role in gamete cell-type specification during embryo sac development (Pagnussat et al., 2009). We believe that *SDG2* activates *SPL/NZZ* expression, forming a key step in the regulatory network of male and female gametophyte development. Nevertheless, *sdg2-1* reduces but does not fully silence *SPL/NZZ* expression, and residual levels of H3K4me3 are detectable at *SPL/NZZ* chromatin in *sdg2-1*, suggesting that additional TrxG family members could be involved in *SPL/NZZ* activation. Moreover, *SDG2* is also required for H3K4me3 deposition and activation of other genes (e.g., *BT3* and *MS1*) which are known to regulate gametophyte development (Ito et al., 2007; Yang et al., 2007; Robert et al., 2009). The fact that *SDG2* regulates several different genes and affects them to varying degrees might account for the variable sporophytic and gametophytic defective phenotypes observed in *sdg2-1* anthers and ovules.

Our study demonstrates that both *SPL/NZZ* and *MS1* are imbedded within a bivalent chromatin domain consisting of transcriptionally active H3K4me3 and transcriptionally repressive H3K27me3 marks. The simultaneous presence of H3K4me3 marked by TrxG and H3K27me3 marked by PcG was first described in mammalian stem cells and was proposed to represent a pluripotent chromatin state that poises genes for

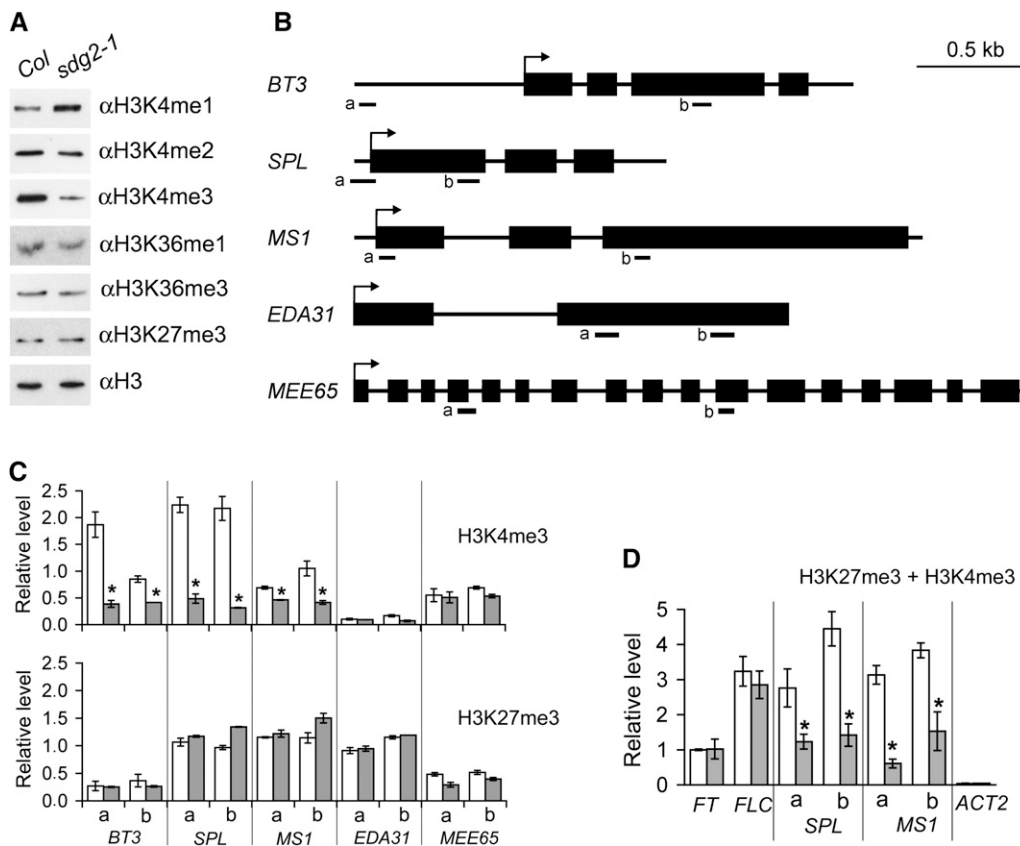


Figure 8. Comparison of Histone Methylation in *sdg2-1* and Col.

(A) Global levels of H3K4, but not H3K36 or H3K27, methylation are perturbed in *sdg2-1* compared with Col. Histone-enriched protein extracts from 20-d-old plants were analyzed by protein immunoblots using specific antibodies that recognize different histone methylation forms as indicated.

(B) Diagram representing genomic structure and ChIP-examined regions of various genes identified as downregulated in *sdg2-1* flower buds. Black boxes represent exons; arrows indicate the ATG start codon sites; bars labeled a or b represent regions amplified by PCR in ChIP analysis.

(C) ChIP analysis of H3K4me3 (top graph) and H3K27me3 (bottom graph) deposition at specific genes in Col (white columns) and *sdg2-1* (gray columns) flower buds. ChIP samples were analyzed by quantitative PCR on two different regions (a and b) of each gene. Relative levels are calculated from mean values of three replicates; error bars show SD. The asterisk indicates a significant difference between *sdg2-1* and Col ($P < 0.01$).

(D) Sequential ChIP analysis for simultaneous presence of H3K27me3 and H3K4me3 at chromatin of specific genes in Col (white columns) and *sdg2-1* (gray columns) flower buds. Chromatin was immunoprecipitated sequentially with anti-H3K27me3 and anti-H3K4me3 antibodies. Quantitative PCR analysis was performed and data shown as described in **(C)**. *FT* and *FLC* serve as positive controls and *ACT2* serves as a negative control.

activation upon appropriate developmental cues (Azuara et al., 2006; Bernstein et al., 2006). In *Arabidopsis*, both TrxG and PcG factors regulate stem cell maintenance genes and floral homeotic genes (reviewed in Shen and Xu, 2009), and the antagonistic function between *ATX1/SDG27* and the PcG gene *CLF* was shown to regulate *AG* expression (Saleh et al., 2007). Currently, however, the most extensively studied TrxG and PcG function is in flowering time regulation (for recent reviews, see He, 2009; Berr and Shen, 2010), and the simultaneous presence of H3K4me3 and H3K27me3 at *FLC* and *FT* has been demonstrated using sequential ChIP analysis (Jiang et al., 2008). *SDG2* is specifically required for marking H3K4me3 for active transcription of *SPL/NZZ* and *MS1* but not *FLC* nor *FT*. The *ATX1/SDG27* and *ATXR7/SDG25* proteins bind *FLC* chromatin (Pien et al., 2008; Tamada et al., 2009). Whether or not the *SDG2* protein directly binds chromatin at *SPL/NZZ* and *MS1* requires future investigation.

The PcG factors involved in H3K27me3 deposition at *SPL/NZZ* and *MS1* chromatin are currently unknown. Future identification of new factors involved in marking H3K27me3 and H3K4me3 at *SPL/NZZ* and *MS1* will be of great interest for understanding regulation of gene expression and the molecular mechanisms underlying male and female gametophyte development.

METHODS

Plant Growth and Mutant Genotyping

Mutant seeds were obtained from the ABRC (<http://www.Arabidopsis.org>): *sdg2-1* (WISCDXSLOX361D10), *sdg2-2* (GK-480F05), *sdg2-3* (SALK_021008), *sdg2-4* (SALK_120450), *sdg2-5* (SALK_138889), *sdg2-6* (SALK_055991), *sdg25-1* (SALK_149692), and *atx1-2* (SALK_149002).

Plants were grown on soil at 21°C under a 16-h-light/8-h-dark photoperiod in a glasshouse. Genotyping was performed by PCR analysis using specific primers (sequences available in Supplemental Table 1 online).

Histochemical Assays and Microscopy

Anther transverse sections were stained with toluidine blue as previously described (Sanders et al., 1999) and visualized by light microscopy. Pollen viability was examined using Alexander's staining solution (Alexander, 1969). DAPI staining was performed by incubation of dissected anthers in a solution containing 0.1% Nonidet P-40, 10% DMSO, 50 mM PIPES, pH 6.9, 5 mM EGTA, and 5 µg/mL DAPI for at least 30 min prior to examination under fluorescence microscopy. For ovule images, pistils were fixed and mounted as previously described (Christensen et al., 1997). Plant organs were examined using a Leica MZ12 dissecting microscope. Higher magnification light and fluorescence images were acquired using a Nikon Eclipse 800 microscope equipped with a CDD camera DXM1200. Confocal plan images were acquired using a Zeiss LSM510 Meta inverted confocal laser microscope (Carl Zeiss). Stacked images were deconvolved to reassign blurred images and subsequently flattened into a single image using ImageJ software and the plug-in DeconvolutionLab (NIH Image). Scanning electron microscopy images were taken using a Hitachi S-3400N (Hitachi High-Technologies Europe). Images were processed with Adobe Photoshop 6.0 (Adobe Systems).

Flow Cytometry

Nuclei were prepared from leaves of 2-week-old plants and stained with propidium iodide as previously described (Galbraith et al., 1983) and analyzed on a FACStar^{PLUS} flow cytometer (BD Biosciences) equipped with an argon laser INNOVA 90-C (Coherent). Propidium iodide fluorescence was excited with 500 mW at 514 nm and measured in the FL1 channel using a 630-nm band-pass filter. A total of 10 to 16 plants were used for each sample, and typically 10,000 nuclei per sample were analyzed. Two replicates were performed for each sample.

In Situ Hybridization

Digoxigenin labeling of RNA probes, tissue preparation, and in situ hybridization was performed as previously described (Zhao et al., 2005). Tissue sections were 8 µm thick. A fragment containing the 396 bp 3'-untranslated region of *SDG2* was obtained by PCR amplification using specific primers (see Supplemental Table 1 online), cloned into the pGEM-T Easy vector (Promega), and used for preparation of the *SDG2* sense (negative control) and antisense probes. Similarly, a fragment containing 359 bp of the 5' region of *SPL/NZZ* was amplified (for primer sequences, see Supplemental Table 1 online), cloned, and used for in situ hybridization.

RT-PCR

RT-PCR was performed using Improm-II reverse transcriptase (Promega) on total RNA extracted from seedlings and various plant organs using the TRIzol kit (Invitrogen) according to the manufacturer's instructions. Gene-specific primers used for PCR amplifications are listed in Supplemental Table 1 online.

For quantitative real-time RT-PCR, gene-specific primers were designed using the LightCycler Probe Design 2 program (Roche) and are listed in Supplemental Table 1 online. Total RNA was isolated from the *sdg2-1* mutant and wild-type flower buds corresponding to developmental stage 8 (Smyth et al., 1990). cDNA was synthesized from 2 µg of total RNA treated with 2 units of DNase I in a total volume of 40 µL using 2 µM oligo(dT)₂₀, 0.5 mM deoxynucleotide triphosphates, 5 mM DTT, and 200 units of SuperScript III reverse transcriptase in 1× first strand buffer

(Invitrogen). A total of 25 to 50 ng cDNA in a total reaction volume of 10 µL SYBR Green Master mix was analyzed using a LightCycler 480 II instrument according to the manufacturer's instructions (Roche). Melting curve analysis was performed to verify amplification of a single PCR product. PCR amplification was performed on three technical replicates on each of the two biological repeat samples. Several conventionally used reference genes were evaluated for their respective stability in our experimental conditions using geNorm (Vandesompele et al., 2002) and Norm Finder (Andersen et al., 2004), and the housekeeping genes *GAPDH*, *TIP41-like*, and *At4g26410* (unknown function) were selected for use as internal references. After normalization with each of the three reference genes, the relative expression level of each gene in the *sdg2-1* mutant was compared with that of the wild type.

Microarray

Total RNA was isolated from *sdg2-1* mutant and wild-type young flower buds corresponding to developmental stage 8 (Smyth et al., 1990), which were pooled from at least 12 individual plants. The microarray analyses were performed using Aligent's Whole *Arabidopsis* Gene Expression Microarray (G2519F, V4, 4x44K) via custom service of the Shanghai Huaguan Biochip Co. All microarray procedures and data analyses were performed according to Aligent's manual (Agilent Technologies). Quantile normalization was performed to make the distribution of probe intensities for each array in a set of arrays the same. Microarray data were deposited at the Gene Expression Omnibus according to "Minimum Information About a Microarray Experiment" standards. Experiments were repeated with independently grown plants, pool of flower buds, RNA preparation, and microarray analysis. Significant genes regulated with a factor of ≥ 2.0 and a P value of ≤ 0.05 in two independent experiments were selected.

Histone Extraction and Immunoblot Analysis

Arabidopsis thaliana histones were extracted from 20-d-old seedlings as previously described (Yu et al., 2004) separated by electrophoresis on 15% SDS-PAGE, and transferred to an Immobilon-P polyvinylidene difluoride transfer membrane (Millipore). Immunoblots were performed using specific antibodies: anti-monomethyl-H3K4 (Upstate Catalog No. 07-436; Millipore), anti-dimethyl H3K4 (Upstate Catalog No. 07-030; Millipore), anti-trimethyl-H3K4 (Upstate Catalog No. 07-473; Millipore), anti-monomethyl-H3K36 (Abcam; ab9048), anti-trimethyl-H3K36 (Abcam; ab9050), anti-trimethyl-H3K27 (Upstate Catalog No. 07-449; Millipore), and anti-H3 (Upstate Catalog No. 05-499; Millipore).

ChIP Analysis

ChIP was performed according to Xu et al. (2008) with the following modifications. Flower buds at developmental stage 8 were used. Chromatin was sheared with a Bioruptor sonicator (Cosmo Bio) twice for 15 min with a 50% duty cycle and high power output to obtain 200- to 1000-bp DNA fragments. Immunoprecipitation was performed using anti-trimethyl-H3K4 or anti-trimethyl-H3K27 antibody together with Protein A-magnetic beads (Millipore). Negative controls were performed without antibody. DNA was recovered using Magna ChIP spin filters according to the manufacturer's instructions (Millipore). ChIP DNA was analyzed by quantitative real-time PCR using gene-specific primers (see Supplemental Table 1 online). Enrichment of H3K4 and H3K27 trimethylation in *sdg2-1* mutant and wild-type flower buds, relative to *ACT2/7* for H3K4me3 and *FUSCA3* for H3K27me3, was calculated using the Pfaffl equation (Pfaffl, 2001).

Sequential ChIP

Sequential ChIP was performed essentially as previously described (Bernstein et al., 2006; Jiang et al., 2008). Briefly, chromatin prepared

from flower buds at developmental stage 8 was first immunoprecipitated with anti-trimethyl-H3K27 antibody and washed, eluted for 30 min at 37°C in 10 mM DTT, and further diluted 1:50 in lysis buffer (Xu et al., 2008). Half of the eluted chromatin was used as a mock control in a second immunoprecipitation without antibody, and the other half was subsequently immunoprecipitated using anti-trimethyl-H3K4 antibody. DNA fragments were recovered and purified for quantitative real-time PCR analysis. Enrichment of bivalent chromatin (with both H3K4me3 and H3K27me3 marks) in *sdg2-1* mutant and wild-type flower buds, relative to the *FT* locus known to be bivalent (Jiang et al., 2008), was calculated using the Pfaffl equation (Pfaffl, 2001). *FLC*, another bivalent locus, and *ACT2/7*, a constitutively expressed locus lacking H3K27 trimethylation, served as positive and negative controls, respectively (Jiang et al., 2008).

Accession Numbers

Sequence data from this article can be found in the Arabidopsis Genome Initiative database under accession number At4g15180 (SDG2). Microarray data can be found at Gene Expression Omnibus (<http://www.ncbi.nlm.nih.gov/geo/>) under accession number GSE18513.

Supplemental Data

The following materials are available in the online version of the article.

Supplemental Figure 1. Comparison of Sections through *sdg2-1* Mutant and Wild-Type Col Flowers.

Supplemental Figure 2. Immunoblot Analysis of H3K4me3 Levels in Col, *sdg2-1*, *sdg25-1*, and *atx1-2*.

Supplemental Table 1. List of Primers Used in This Study.

Supplemental Data Set 1A. List of Genes Downregulated by More Than Twofold in *sdg2-1* Compared with Wild-Type Flower Buds around Developmental Stage 8.

Supplemental Data Set 1B. List of Genes Upregulated by More Than Twofold in *sdg2-1* Compared with Wild-Type Flower Buds around Developmental Stage 8.

ACKNOWLEDGMENTS

We thank L. Xu and M.F. Mbengue for assistance in early stages of *sdg2* mutant identification, M. Erhardt for assistance in microscopy analysis, and A. Alioua for assistance in quantitative PCR analysis. This work was supported in part by the Centre National de la Recherche Scientifique and Agence Nationale de la Recherche (ANR 06-BLAN-0054-01).

Received September 28, 2010; revised September 28, 2010; accepted October 13, 2010; published October 29, 2010.

REFERENCES

- Aarts, M.G., Hodge, R., Kalantidis, K., Florack, D., Wilson, Z.A., Mulligan, B.J., Stiekema, W.J., Scott, R., and Pereira, A. (1997). The *Arabidopsis* MALE STERILITY 2 protein shares similarity with reductases in elongation/condensation complexes. *Plant J.* **12**: 615–623.
- Alexander, M.P. (1969). Differential staining of aborted and nonaborted pollen. *Stain Technol.* **44**: 117–122.
- Alvarez-Venegas, R., and Avramova, Z. (2005). Methylation patterns of histone H3 Lys 4, Lys 9 and Lys 27 in transcriptionally active and inactive *Arabidopsis* genes and in *atx1* mutants. *Nucleic Acids Res.* **33**: 5199–5207.
- Alvarez-Venegas, R., Pien, S., Sadler, M., Witmer, X., Grossniklaus, U., and Avramova, Z. (2003). ATX-1, an *Arabidopsis* homolog of trithorax, activates flower homeotic genes. *Curr. Biol.* **13**: 627–637.
- Alves-Ferreira, M., Wellmer, F., Banhara, A., Kumar, V., Riechmann, J.L., and Meyerowitz, E.M. (2007). Global expression profiling applied to the analysis of *Arabidopsis* stamen development. *Plant Physiol.* **145**: 747–762.
- Andersen, C.L., Jensen, J.L., and Ørntoft, T.F. (2004). Normalization of real-time quantitative reverse transcription-PCR data: A model-based variance estimation approach to identify genes suited for normalization, applied to bladder and colon cancer data sets. *Cancer Res.* **64**: 5245–5250.
- Azuara, V., Perry, P., Sauer, S., Spivakov, M., Jørgensen, H.F., John, R.M., Gouti, M., Casanova, M., Warnes, G., Merckenschlager, M., and Fisher, A.G. (2006). Chromatin signatures of pluripotent cell lines. *Nat. Cell Biol.* **8**: 532–538.
- Balasubramanian, S., and Schneitz, K. (2000). NOZZLE regulates proximal-distal pattern formation, cell proliferation and early sporogenesis during ovule development in *Arabidopsis thaliana*. *Development* **127**: 4227–4238.
- Balasubramanian, S., and Schneitz, K. (2002). NOZZLE links proximal-distal and adaxial-abaxial pattern formation during ovule development in *Arabidopsis thaliana*. *Development* **129**: 4291–4300.
- Barow, M., and Meister, A. (2003). Endopolyploidy in seed plants is differently correlated to systematics, organ, life strategy and genome size. *Plant Cell Environ.* **26**: 571–584.
- Baubec, T., Dinh, H.Q., Pecinka, A., Rakic, B., Rozhon, W., Wohlrab, B., von Haeseler, A., and Mittelsten Scheid, O. (2010). Cooperation of multiple chromatin modifications can generate unanticipated stability of epigenetic states in *Arabidopsis*. *Plant Cell* **22**: 34–47.
- Baumbusch, L.O., Thorstensen, T., Krauss, V., Fischer, A., Naumann, K., Assalkhou, R., Schulz, I., Reuter, G., and Aalen, R.B. (2001). The *Arabidopsis thaliana* genome contains at least 29 active genes encoding SET domain proteins that can be assigned to four evolutionarily conserved classes. *Nucleic Acids Res.* **29**: 4319–4333.
- Bernstein, B.E., et al. (2006). A bivalent chromatin structure marks key developmental genes in embryonic stem cells. *Cell* **125**: 315–326.
- Berr, A., and Shen, W.H. (2010). Molecular mechanisms in epigenetic regulation of plant growth and development. In *Plant Developmental Biology—Biotechnological Perspectives*, Vol. 2, E.-C. Pua and M.R. Davey, eds (Berlin/Heidelberg: Springer-Verlag), pp. 325–344.
- Berr, A., Xu, L., Gao, J., Cognat, V., Steinmetz, A., Dong, A., and Shen, W.H. (2009). SET DOMAIN GROUP25 encodes a histone methyltransferase and is involved in FLOWERING LOCUS C activation and repression of flowering. *Plant Physiol.* **151**: 1476–1485.
- Boavida, L.C., Shuai, B., Yu, H.J., Pagnussat, G.C., Sundaresan, V., and McCormick, S. (2009). A collection of *Ds* insertional mutants associated with defects in male gametophyte development and function in *Arabidopsis thaliana*. *Genetics* **181**: 1369–1385.
- Borde, V., Robine, N., Lin, W., Bonfils, S., Géli, V., and Nicolas, A. (2009). Histone H3 lysine 4 trimethylation marks meiotic recombination initiation sites. *EMBO J.* **28**: 99–111.
- Borges, F., Gomes, G., Gardner, R., Moreno, N., McCormick, S., Feijó, J.A., and Becker, J.D. (2008). Comparative transcriptomics of *Arabidopsis* sperm cells. *Plant Physiol.* **148**: 1168–1181.
- Bowman, J.L., Smyth, D.R., and Meyerowitz, E.M. (1989). Genes directing flower development in *Arabidopsis*. *Plant Cell* **1**: 37–52.
- Bowman, J.L., Smyth, D.R., and Meyerowitz, E.M. (1991). Genetic interactions among floral homeotic genes of *Arabidopsis*. *Development* **112**: 1–20.
- Canales, C., Bhatt, A.M., Scott, R., and Dickinson, H. (2002). EXS, a

- putative LRR receptor kinase, regulates male germline cell number and tapetal identity and promotes seed development in *Arabidopsis*. *Curr. Biol.* **12**: 1718–1727.
- Cartagena, J.A., Matsunaga, S., Seki, M., Kurihara, D., Yokoyama, M., Shinozaki, K., Fujimoto, S., Azumi, Y., Uchiyama, S., and Fukui, K.** (2008). The *Arabidopsis* *SDG4* contributes to the regulation of pollen tube growth by methylation of histone H3 lysines 4 and 36 in mature pollen. *Dev. Biol.* **315**: 355–368.
- Cazzonelli, C.I., Cuttriss, A.J., Cossetto, S.B., Pye, W., Crisp, P., Whelan, J., Finnegan, E.J., Turnbull, C., and Pogson, B.J.** (2009). Regulation of carotenoid composition and shoot branching in *Arabidopsis* by a chromatin modifying histone methyltransferase, *SDG8*. *Plant Cell* **21**: 39–53.
- Christensen, C.A., King, E.J., Jordan, J.R., and Drews, G.N.** (1997). Megagametogenesis in *Arabidopsis* wild type and *Gf* mutant. *Sex. Plant Reprod.* **10**: 49–64.
- Galbraith, D.W., Harkins, K.R., Maddox, J.M., Ayres, N.M., Sharma, D.P., and Firoozabady, E.** (1983). Rapid flow cytometric analysis of the cell cycle in intact plant tissues. *Science* **220**: 1049–1051.
- Grini, P.E., Thorstensen, T., Alm, V., Vizcay-Barrena, G., Windju, S.S., Jørstad, T.S., Wilson, Z.A., and Aalen, R.B.** (2009). The ASH1 HOMOLOG 2 (*ASHH2*) histone H3 methyltransferase is required for ovule and anther development in *Arabidopsis*. *PLoS ONE* **4**: e7817.
- Hayashi, K., Yoshida, K., and Matsui, Y.** (2005). A histone H3 methyltransferase controls epigenetic events required for meiotic prophase. *Nature* **438**: 374–378.
- He, Y.** (2009). Control of the transition to flowering by chromatin modifications. *Mol. Plant* **2**: 554–564.
- Hochwagen, A., and Marais, G.A.** (2010). Meiosis: A PRDM9 guide to the hotspots of recombination. *Curr. Biol.* **20**: R271–R274.
- Inzé, D., and De Veylder, L.** (2006). Cell cycle regulation in plant development. *Annu. Rev. Genet.* **40**: 77–105.
- Ito, T., Nagata, N., Yoshida, Y., Ohme-Takagi, M., Ma, H., and Shinozaki, K.** (2007). *Arabidopsis* *MALE STERILITY1* encodes a PHD-type transcription factor and regulates pollen and tapetum development. *Plant Cell* **19**: 3549–3562.
- Ito, T., Wellmer, F., Yu, H., Das, P., Ito, N., Alves-Ferreira, M., Riechmann, J.L., and Meyerowitz, E.M.** (2004). The homeotic protein *AGAMOUS* controls microsporogenesis by regulation of *SPOROCYTELESS*. *Nature* **430**: 356–360.
- Jiang, D., Wang, Y., Wang, Y., and He, Y.** (2008). Repression of *FLOWERING LOCUS C* and *FLOWERING LOCUS T* by the *Arabidopsis* Polycomb repressive complex 2 components. *PLoS ONE* **3**: e3404.
- Kim, S.Y., He, Y., Jacob, Y., Noh, Y.S., Michaels, S., and Amasino, R.** (2005). Establishment of the vernalization-responsive, winter-annual habit in *Arabidopsis* requires a putative histone H3 methyl transferase. *Plant Cell* **17**: 3301–3310.
- Kondrosi, E., Roudier, F., and Gendreau, E.** (2000). Plant cell-size control: Growing by ploidy? *Curr. Opin. Plant Biol.* **3**: 488–492.
- Lee, H.S., and Chen, Z.J.** (2001). Protein-coding genes are epigenetically regulated in *Arabidopsis* polyploids. *Proc. Natl. Acad. Sci. USA* **98**: 6753–6758.
- Lenhard, M., Bohnert, A., Jürgens, G., and Laux, T.** (2001). Termination of stem cell maintenance in *Arabidopsis* floral meristems by interactions between *WUSCHEL* and *AGAMOUS*. *Cell* **105**: 805–814.
- Li, L.C., Qin, G.J., Tsuge, T., Hou, X.H., Ding, M.Y., Aoyama, T., Oka, A., Chen, Z., Gu, H., Zhao, Y., and Qu, L.J.** (2008). *SPOROCYTELESS* modulates *YUCCA* expression to regulate the development of lateral organs in *Arabidopsis*. *New Phytol.* **179**: 751–764.
- Liu, C., Lu, F., Cui, X., and Cao, X.** (2010). Histone methylation in higher plants. *Annu. Rev. Plant Biol.* **61**: 395–420.
- Liu, X., Huang, J., Parameswaran, S., Ito, T., Seubert, B., Auer, M., Rymaszewski, A., Jia, G., Owen, H.A., and Zhao, D.** (2009). The *SPOROCYTELESS/NOZZLE* gene is involved in controlling stamen identity in *Arabidopsis*. *Plant Physiol.* **151**: 1401–1411.
- Lohmann, J.U., Hong, R.L., Hobe, M., Busch, M.A., Parcy, F., Simon, R., and Weigel, D.** (2001). A molecular link between stem cell regulation and floral patterning in *Arabidopsis*. *Cell* **105**: 793–803.
- Ma, H.** (2005). Molecular genetic analyses of microsporogenesis and microgametogenesis in flowering plants. *Annu. Rev. Plant Biol.* **56**: 393–434.
- Ng, D.W., Wang, T., Chandrasekharan, M.B., Aramayo, R., Kertbundit, S., and Hall, T.C.** (2007). Plant SET domain-containing proteins: structure, function and regulation. *Biochim. Biophys. Acta* **1769**: 316–329.
- Pagnussat, G.C., Alandete-Saez, M., Bowman, J.L., and Sundaresan, V.** (2009). Auxin-dependent patterning and gamete specification in the *Arabidopsis* female gametophyte. *Science* **324**: 1684–1689.
- Pagnussat, G.C., Yu, H.J., Ngo, Q.A., Rajani, S., Mayalagu, S., Johnson, C.S., Capron, A., Xie, L.F., Ye, D., and Sundaresan, V.** (2005). Genetic and molecular identification of genes required for female gametophyte development and function in *Arabidopsis*. *Development* **132**: 603–614.
- Pfaffl, M.W.** (2001). A new mathematical model for relative quantification in real-time RT-PCR. *Nucleic Acids Res.* **29**: e45.
- Pien, S., Fleury, D., Mylne, J.S., Crevillen, P., Inzé, D., Avramova, Z., Dean, C., and Grossniklaus, U.** (2008). *ARABIDOPSIS TRITHORAX1* dynamically regulates *FLOWERING LOCUS C* activation via histone 3 lysine 4 trimethylation. *Plant Cell* **20**: 580–588.
- Robert, H.S., Quint, A., Brand, D., Vivian-Smith, A., and Offringa, R.** (2009). BTB AND TAZ DOMAIN scaffold proteins perform a crucial function in *Arabidopsis* development. *Plant J.* **58**: 109–121.
- Rotman, N., Durberry, A., Wardle, A., Yang, W.C., Chaboud, A., Faure, J.E., Berger, F., and Twell, D.** (2005). A novel class of MYB factors controls sperm-cell formation in plants. *Curr. Biol.* **15**: 244–248.
- Saleh, A., Al-Abdallat, A., Ndamukong, I., Alvarez-Venegas, R., and Avramova, Z.** (2007). The *Arabidopsis* homologs of trithorax (*ATX1*) and enhancer of zeste (*CLF*) establish ‘bivalent chromatin marks’ at the silent *AGAMOUS* locus. *Nucleic Acids Res.* **35**: 6290–6296.
- Saleh, A., Alvarez-Venegas, R., Yilmaz, M., Le, O., Hou, G., Sadler, M., Al-Abdallat, A., Xia, Y., Lu, G., Ladunga, I., and Avramova, Z.** (2008). The highly similar *Arabidopsis* homologs of trithorax *ATX1* and *ATX2* encode proteins with divergent biochemical functions. *Plant Cell* **20**: 568–579.
- Sanders, P.M., Bui, A.Q., Weterings, K., McIntire, K.N., Hsu, Y.C., Lee, P.Y., Truong, M.T., Beals, T.P., and Goldberg, R.B.** (1999). Anther developmental defects in *Arabidopsis thaliana* male sterile mutants. *Sex. Plant Reprod.* **11**: 297–322.
- Schiefthaler, U., Balasubramanian, S., Sieber, P., Chevalier, D., Wisman, E., and Schneitz, K.** (1999). Molecular analysis of *NOZZLE*, a gene involved in pattern formation and early sporogenesis during sex organ development in *Arabidopsis thaliana*. *Proc. Natl. Acad. Sci. USA* **96**: 11664–11669.
- Schuettengruber, B., Chourrout, D., Vervoort, M., Leblanc, B., and Cavalli, G.** (2007). Genome regulation by polycomb and trithorax proteins. *Cell* **128**: 735–745.
- Shen, W.H., and Xu, L.** (2009). Chromatin remodeling in stem cell maintenance in *Arabidopsis thaliana*. *Mol. Plant* **2**: 600–609.
- Sieber, P., Petrascheck, M., Barberis, A., and Schneitz, K.** (2004). Organ polarity in *Arabidopsis*. *NOZZLE* physically interacts with members of the *YABBY* family. *Plant Physiol.* **135**: 2172–2185.
- Smyth, D.R., Bowman, J.L., and Meyerowitz, E.M.** (1990). Early flower development in *Arabidopsis*. *Plant Cell* **2**: 755–767.
- Soppe, W.J., Bentsink, L., and Koornneef, M.** (1999). The early-flowering

- mutant *efs* is involved in the autonomous promotion pathway of *Arabidopsis thaliana*. *Development* **126**: 4763–4770.
- Springer, N.M., Napoli, C.A., Selinger, D.A., Pandey, R., Cone, K.C., Chandler, V.L., Kaeppler, H.F., and Kaeppler, S.M.** (2003). Comparative analysis of SET domain proteins in maize and *Arabidopsis* reveals multiple duplications preceding the divergence of monocots and dicots. *Plant Physiol.* **132**: 907–925.
- Tamada, Y., Yun, J.Y., Woo, S.C., and Amasino, R.M.** (2009). *ARABIDOPSIS TRITHORAX-RELATED7* is required for methylation of lysine 4 of histone H3 and for transcriptional activation of *FLOWERING LOCUS C*. *Plant Cell* **21**: 3257–3269.
- Thorstensen, T., Grini, P.E., Mercy, I.S., Alm, V., Erdal, S., Aasland, R., and Aalen, R.B.** (2008). The *Arabidopsis* SET-domain protein ASHR3 is involved in stamen development and interacts with the bHLH transcription factor ABORTED MICROSPORES (AMS). *Plant Mol. Biol.* **66**: 47–59.
- Tschiersch, B., Hofmann, A., Krauss, V., Dorn, R., Korge, G., and Reuter, G.** (1994). The protein encoded by the *Drosophila* position-effect variegation suppressor gene *Su(var)3-9* combines domains of antagonistic regulators of homeotic gene complexes. *EMBO J.* **13**: 3822–3831.
- Vandesompele, J., De Preter, K., Pattyn, F., Poppe, B., Van Roy, N., De Paepe, A., and Speleman, F.** (2002). Accurate normalization of real-time quantitative RT-PCR data by geometric averaging of multiple internal control genes. *Genome Biol.* **3**: RESEARCH0034.
- Wijeratne, A.J., Zhang, W., Sun, Y., Liu, W., Albert, R., Zheng, Z., Oppenheimer, D.G., Zhao, D., and Ma, H.** (2007). Differential gene expression in *Arabidopsis* wild-type and mutant anthers: insights into anther cell differentiation and regulatory networks. *Plant J.* **52**: 14–29.
- Wilson, Z.A., and Zhang, D.B.** (2009). From *Arabidopsis* to rice: Pathways in pollen development. *J. Exp. Bot.* **60**: 1479–1492.
- Wuest, S.E., Vijverberg, K., Schmidt, A., Weiss, M., Gheyselinck, J., Lohr, M., Wellmer, F., Rahnenführer, J., von Mering, C., and Grossniklaus, U.** (2010). *Arabidopsis* female gametophyte gene expression map reveals similarities between plant and animal gametes. *Curr. Biol.* **20**: 506–512.
- Xu, L., Zhao, Z., Dong, A., Soubigou-Taconnat, L., Renou, J.P., Steinmetz, A., and Shen, W.H.** (2008). Di- and tri- but not mono-methylation on histone H3 lysine 36 marks active transcription of genes involved in flowering time regulation and other processes in *Arabidopsis thaliana*. *Mol. Cell. Biol.* **28**: 1348–1360.
- Yang, C., Vizcay-Barrena, G., Conner, K., and Wilson, Z.A.** (2007). *MALE STERILITY1* is required for tapetal development and pollen wall biosynthesis. *Plant Cell* **19**: 3530–3548.
- Yang, S.L., Xie, L.F., Mao, H.Z., Pua, C.S., Yang, W.C., Jiang, L., Sundaresan, V., and Ye, D.** (2003). *TAPETUM DETERMINANT1* is required for cell specialization in the *Arabidopsis* anther. *Plant Cell* **15**: 2792–2804.
- Yang, W.C., Shi, D.Q., and Chen, Y.H.** (2010). Female gametophyte development in flowering plants. *Annu. Rev. Plant Biol.* **61**: 89–108.
- Yang, W.C., Ye, D., Xu, J., and Sundaresan, V.** (1999). The *SPORO-CYTELESS* gene of *Arabidopsis* is required for initiation of sporogenesis and encodes a novel nuclear protein. *Genes Dev.* **13**: 2108–2117.
- Yu, H.J., Hogan, P., and Sundaresan, V.** (2005). Analysis of the female gametophyte transcriptome of *Arabidopsis* by comparative expression profiling. *Plant Physiol.* **139**: 1853–1869.
- Yu, Y., Dong, A., and Shen, W.H.** (2004). Molecular characterization of the tobacco SET domain protein NtSET1 unravels its role in histone methylation, chromatin binding, and segregation. *Plant J.* **40**: 699–711.
- Yu, Y., Pu, Z., Shen, W.H., and Dong, A.** (2009). An update on histone lysine methylation in plants. *Prog. Nat. Sci.* **19**: 407–413.
- Zhang, W., Sun, Y., Timofejeva, L., Chen, C., Grossniklaus, U., and Ma, H.** (2006). Regulation of *Arabidopsis* tapetum development and function by *DYSFUNCTIONAL TAPETUM1 (DYT1)* encoding a putative bHLH transcription factor. *Development* **133**: 3085–3095.
- Zhang, X., Bernatavichute, Y.V., Cokus, S., Pellegrini, M., and Jacobsen, S.E.** (2009). Genome-wide analysis of mono-, di- and trimethylation of histone H3 lysine 4 in *Arabidopsis thaliana*. *Genome Biol.* **10**: R62.
- Zhang, Z.B., et al.** (2007). Transcription factor AtMYB103 is required for anther development by regulating tapetum development, callose dissolution and exine formation in *Arabidopsis*. *Plant J.* **52**: 528–538.
- Zhao, D.Z., Wang, G.F., Speal, B., and Ma, H.** (2002). The *EXCESS MICROSPOROCYTES1* gene encodes a putative leucine-rich repeat receptor protein kinase that controls somatic and reproductive cell fates in the *Arabidopsis* anther. *Genes Dev.* **16**: 2021–2031.
- Zhao, Z., and Shen, W.H.** (2004). Plants contain a high number of proteins showing sequence similarity to the animal SUV39H family of histone methyltransferases. *Ann. N. Y. Acad. Sci.* **1030**: 661–669.
- Zhao, Z., Yu, Y., Meyer, D., Wu, C., and Shen, W.H.** (2005). Prevention of early flowering by expression of *FLOWERING LOCUS C* requires methylation of histone H3 K36. *Nat. Cell Biol.* **7**: 1256–1260.